# Transient picometer atomic displacements in α-Te photoexcited by femtosecond laser pulses

Sergey I. Kudryashov,[1)] Maria Kandyla,[2)] Chris A. Roeser,[2)] Eric Mazur[3)]

[1)] P.N. Lebedev Physical Institute, Russian Academy of Science, 119991 Moscow, Russia
[2)] Massachusetts Institute of Technology, Lexington, MA 02420, USA
[3)] Department of Physics and Division of Engineering and Applied Sciences, Harvard University, Cambridge, MA 02138, USA

## ABSTRACT

Subpicosecond, picometer atomic displacements in α-Te photoexcited by single femtosecond laser pulses have been measured by means of time-resolved optical reflectometry revealing threshold-like coherent quantum emission of single softened fully symmetrical optical $A_1$-phonons and demonstrating absolute detection capability of this technique in studies of coherent phonon dynamics in solids.

**Keywords:** ultrashort (femtosecond) laser pulses; α-Te; coherent optical phonons; sub-picosecond picometer atomic displacements

## I. INTRODUCTION

The invention of femtosecond (fs) lasers in the early 80s enabled experimental studies of excitation and dynamics of electron–hole plasma-driven coherent optical phonons in semiconductors, semimetals and metals,[1-5] corresponding to sub-picosecond sub-lattice oscillations in their crystalline structures. The phonons manifest themselves in quasi-periodic oscillations of the isotropic or the anisotropic optical reflectivity of the absorbing materials at the optical phonon frequency Ω because of modulation of their bandstructure.[3,6] The background component on which the oscillations are superimposed includes screening, exchange, correlation and Drude gas contributions to the bandgap renormalization from the electron-hole plasma (EHP) created by photoexcitation.[7] It also includes a contribution from a quasi-static displacement of ion sub-lattices towards a new EHP-defined position of equilibrium.[1,6] Surprisingly, the displacement direction was shown to lead to a more symmetric crystalline structure, usually a metallic Peierls phase.[4,8] At high electronic excitation levels coherent optical phonons exhibit considerable (up to 20%) EHP-induced softening, related to reduced Ω.[3-5] The EHP-driven excitation and softening of the coherent optical phonons and the phonon-induced bandgap shrinkage in many semiconductors and semimetals seems to represent an initial stage of *dynamic* displacive Peierls (Jan-Teller) structural distortions due to deformation-potential electron,hole - optical phonon (e,h-phonon) coupling.[8] Also, specific softened coherent optical phonons may be precursors of corresponding operative "soft" phonon modes.

There are relatively few experimental techniques capable of visualizing directly or indirectly coherent phonon dynamics in insulating solids, e.g., time-domain techniques as time-resolved X-ray diffraction (XRD)[4,8,9] and electron diffraction (ED),[10] or time-resolved optical reflectometry (OR, both linear[1-3,5-5] and non-linear variants[11]) and two-photon photoemission spectroscopy (PES)[12], respectively. However, current acquisition capabilities of these techniques are not always sufficient for studying ultrafast low-amplitude coherent phonon dynamics with minimal oscillation periods $T > 10^{-14}$ s and amplitudes $U > 10^{-12}$ m. To date, XRD techniques demonstrated quite high temporal resolution (150 fs[9]) and sensitivity (10-20 pm[4]), which are somewhat better than the similar parameters of ED techniques (~400 fs[10] and 10-30 pm[10]). In contrast, the available OR and PES techniques exhibit maximum temporal resolution close to minimal femtosecond laser pulse widths of ~10 fs, while the claimed estimated sensitivity approaches to a single-phonon amplitude of 1 pm[12] (note that emission of single coherent phonons has not been resolved in the latter study and quantitative interpre-

ICONO 2007: Nonlinear Laser Spectroscopy and High-Precision Measurements; and Fundamentals of Laser Chemistry and Biophotonics, edited by Sergey Tikhomirov, Thomas Udem, Valery Yudin, Maxim Pshenichnikov, Oleg Sarkisov, Proc. of SPIE Vol. 6727, 672709, (2007) · 0277-786X/07/$18 · doi: 10.1117/12.752233

tation of experimental results is not straightforward).
In this study we report on time-resolved (pump/probe) reflection measurements of transient picometer displacements of atomic sub-lattices in α-Te photoexcited by single 30-fs IR femtosecond pulses of variable energy. The oscillatory reflectivity transients obtained with 30-fs temporal resolution exhibit picosecond-long modulation of the materials dielectric function at the characteristic frequencies of 3.2-3.5 THz representing coherent softened fully symmetrical optical phonon $A_1$. Separating the oscillatory component of the modulation from quasi-static purely electronic and lattice components, the oscillation amplitude was obtained as a function of surface electron-hole plasma density calculated using the corresponding laser pulse energies. This dependence exhibits threshold-like coherent quantum emission of single (1-4 phonons) $A_1$-phonons with their amplitudes increasing in the range of 4-10 pm as a function of electronic excitation level demonstrating the absolute detection sensitivity and very high temporal resolution achieved with this measurement technique in coherent phonon studies.

## II. EXPERIMENTAL SETUP AND TECHNIQUE

A dual-angle-of-incidence pump-probe reflectometry technique has been developed to measure experimentally the dielectric function of α-Te with femtosecond time resolution.[13] Pump–probe experiments were performed on a single-crystal Czochralski-grown tellurium sample using 800-nm pulses from a multi-pass amplified Ti:sapphire laser, producing 0.5-mJ, 35-fs pulses at a repetition rate of 1 kHz.[14]
An *s*-polarized pump pulse excites the sample at different absorbed (non-reflected) peak laser fluences $F_{abs}$ below the threshold for permanent visible damage, $F_{th} = 2.1$ mJ/cm$^2$, while the *p*-polarized transient reflectivity is measured using a white-light pulse ($\hbar\omega = 1.65–3.2$ eV) (Fig.1). Two-photon absorption measurements[15] indicate that the time-resolution of the pump-probe setup is better than 50 fs, while calculations based on measurements of the spectrum and chirp of the white-light probe indicate that the time resolution of the probe varies from 20 fs near 1.7 eV to 60 fs near 3.2 eV.[16] The entire system is calibrated to obtain absolute reflectivity.

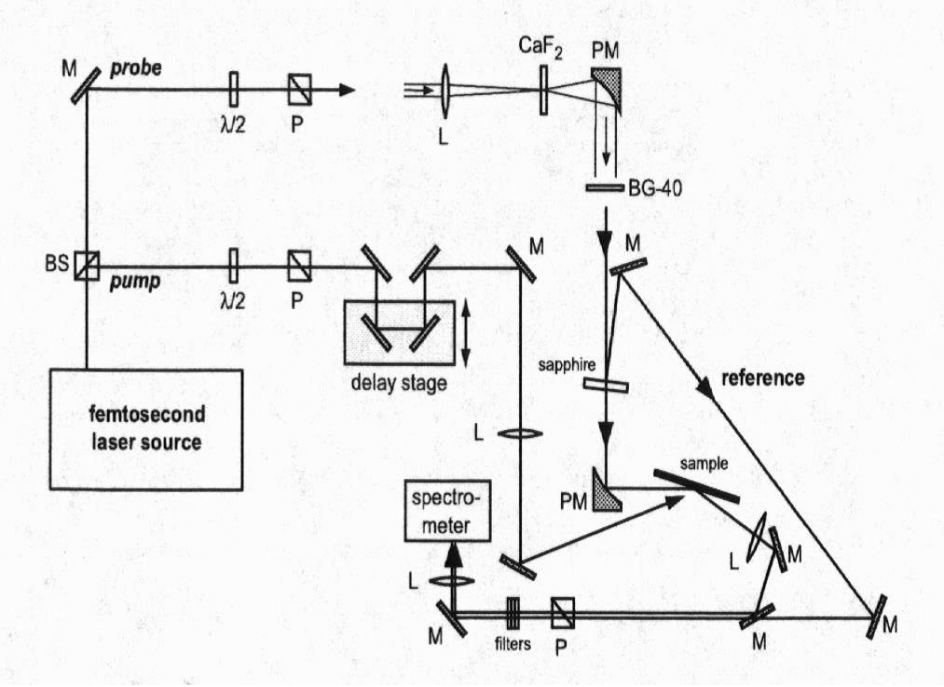


Fig.1 (left). Experimental setup for pump/probe measurements (see details in the text; after [17]).

Spectral reflectivity measurements at 68.4° and 80.4° angle of incidence, with the optic axis of Te, ***c***, perpendicular to the plane of incidence of the probe ("ordinary" probing and "extraordinary" pumping electric fields, $\boldsymbol{E}_{\mathbf{pr}} \perp \boldsymbol{c}$ and $\boldsymbol{E}_{\mathbf{pu}} \parallel \boldsymbol{c}$), allow us to determine the ordinary dielectric function $\varepsilon_{ord}(\omega)$ (Fig.2). Measurements at the same two angles of incidence with the sample rotated so the optic axis ***c*** lied within the probe plane of incidence ("extraordinary" probing and "ordinary" pumping electric fields $\boldsymbol{E}_{\mathbf{pr}} \parallel \boldsymbol{c}$ and $\boldsymbol{E}_{\mathbf{pu}} \perp \boldsymbol{c}$), allow extraction of the extraordinary dielectric function $\varepsilon_{ext}(\omega)$, given measured values of $\varepsilon_{ord}(\omega)$ at each time delay. For negative time delays, when the probe arrives before the pump, the extracted $\varepsilon_{ord}(\omega)$ and $\varepsilon_{ext}(\omega)$ are in excellent agreement with corresponding literature data.[18] Further details of this experimental technique can be found in Refs.[3,13].

The resulting experimental spectral dependence of $\varepsilon_{ord}(\omega)$ and $\varepsilon_{ext}(\omega)$ on the probe frequency $\omega$ (Fig.3) can be fitted well using the Drude-Lorentz model[19]

$$\varepsilon(\omega) = \frac{Ne^2}{\varepsilon_0 m} \frac{1}{\omega_{res}^2 - \omega^2 - i\omega\Gamma}, \qquad (1)$$

extracting at each time delay the resonance energy $E_{res} = \hbar\omega_{res}$ (in equilibrium $E_{res,ord} \approx 2.3$ eV, $E_{res,ext} \approx 2.1$ eV), while the resonance linewidth $\hbar\Gamma$, and the oscillator strength $f = Ne^2/\varepsilon_0 m$ are considered as free parameters. Resonances outside the spectral range of the probe give roughly constant contributions to the real part of the dielectric function within the probe range, so a real additive constant $C$ was included in the fit to $\varepsilon_{ord}(\omega)$ and $\varepsilon_{ext}(\omega)$ to account for this offset.

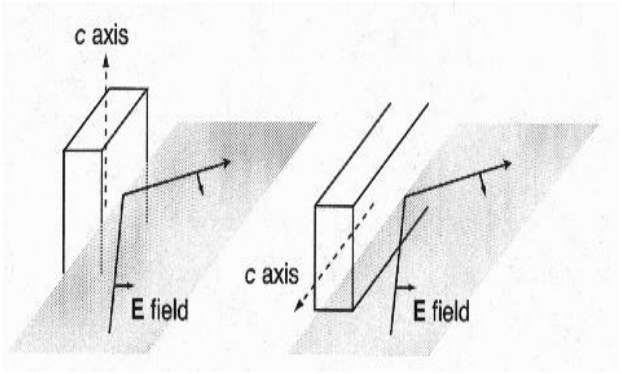


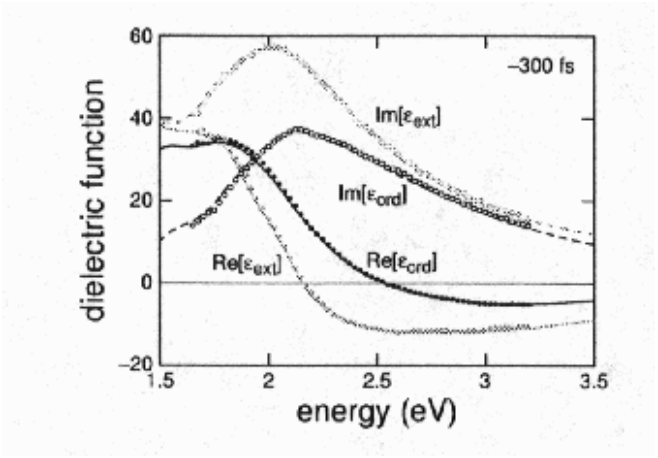


Fig. 2 (left). Probing geometries in α-Te used in this work (after[17]).

Fig.3 (right). Spectral dependence of $\varepsilon_{ord}(\omega)$ and $\varepsilon_{ext}(\omega)$ on the probe frequency $\omega$ for unexcited α-Te at negative delay of 300 fs. Lines and symbols represent literature data[18] and experimental data of this work, respectively.

## III. EXPERIMENTAL RESULTS

Figure 4 shows the transient behavior of the resonance energies $E_{res,ord}$ and $E_{res,ext}$ at $F_{abs} = 0.85F_{th}$ with respect to their equilibrium values. Each resonance energy redshifts because of a transient bandgap renormalization by $\Delta E_{res}(t) = [E_{res}(t<0) - E_{res}(t)]$ reaching at time delays $t \approx 0.1$-0.3 ps its maximum redshift value, $|\Delta E_{res}|$, and oscillates at a time- and fluence-dependent frequency $\Omega < \Omega_0(295\text{ K})$, where $\Omega_0(295\text{ K}) \approx 3.6$ THz is the $A_1$-phonon frequency in α-Te at ambient temperature of 295 K.[20] In Figure 5 we present the dependence of $\Omega_{ord}$ and $\Omega_{ext}$ on $F_{abs}$, which was obtained by extrapolation of the experimental transients $\Omega_{ord}(t)$ and $\Omega_{ext}(t)$ for $t \approx 0.3$-2 ps and for different $F_{abs}$ values to $t \approx 0.1$ ps. It is only these $\Omega_{ord,ext}(t \approx 0.1\text{ ps})$ values that we will consider throughout this work.

The maximum negative bandgap renormalization (redshift) of the resonance energies, $|\Delta E_{res}|$, which is reached at very early time delays $t \approx 0.1$-0.3 ps, consists presumably of two non-thermal contributions (at negligible thermal effects) arising from purely electronic screening, exchange and correlation effects in EHP (electronic part $|\Delta E_{res}^{ee}|$) and from the

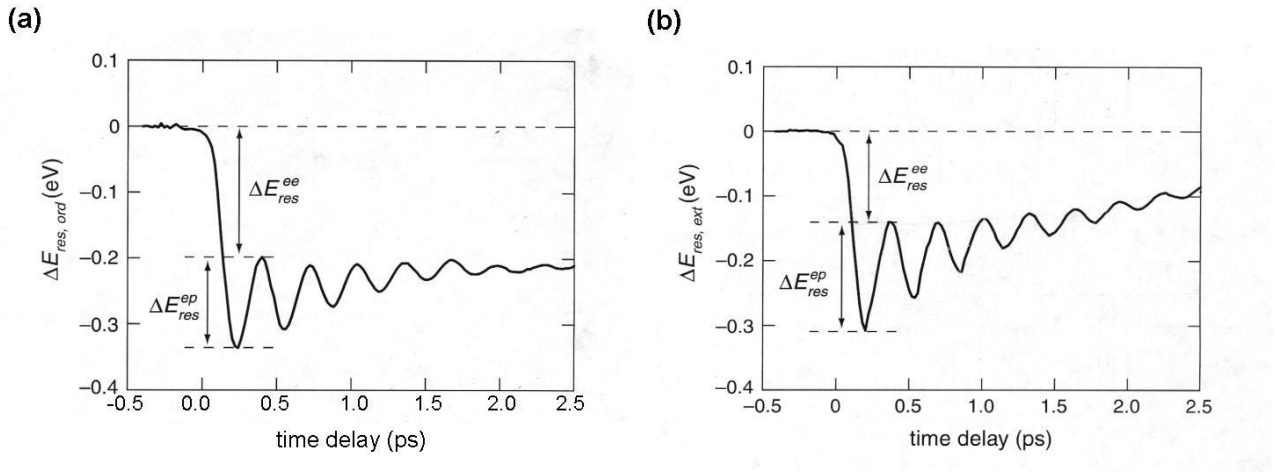


Fig. 4. Transient shifts of the resonance energy $E_{res}(t)$ in α-Te with respect to $E_{res}(t < 0)$ shown by the horizontal dotted line, for ordinary $\varepsilon_{ord}$ (*a*) and extraordinary $\varepsilon_{ext}$ (*b*) dielectric functions at absorbed laser fluence $F_{abs} = 0.85F_{th}$. Transient electronic and phonon-induced bandgap renormalization magnitudes, $\Delta E_{res}^{ee}$ and $\Delta E_{res}^{ep}$, respectively, are shown by arrows.

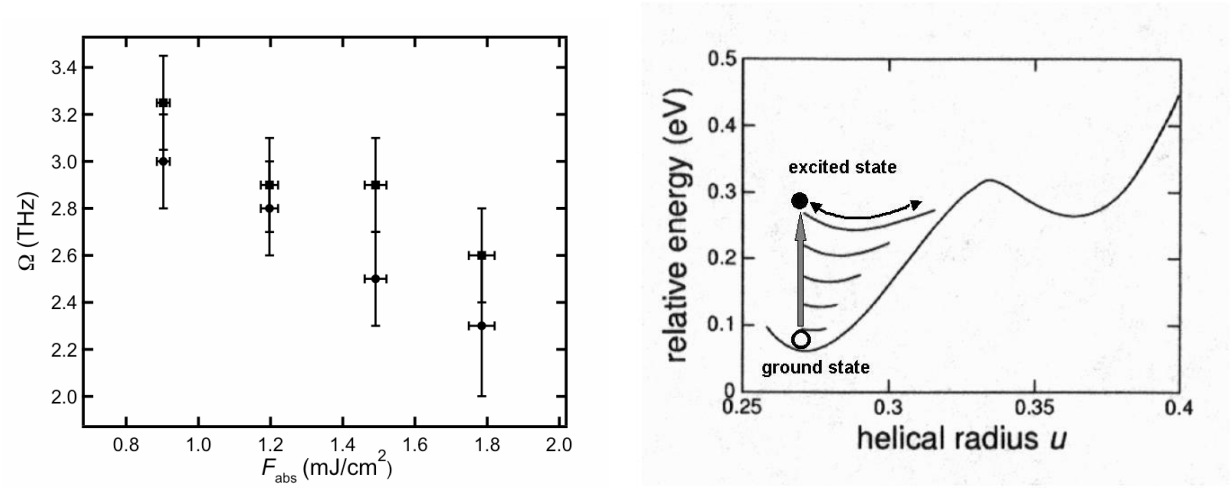


Fig.5 (left). $A_1$-phonon oscillation frequency Ω in α-Te, derived by Short Fourier Transformation on the quasi-harmonic spectral shifts of the resonance energy of $\varepsilon_{ord}$ (circles) and $\varepsilon_{ext}$ (squares) and extrapolated to $t \approx 0.1$ ps, vs. $F_{abs}$. Crosses around symbols show the error bars of the extrapolation process used.

Fig. 6 (right). Potential curves of excited states in α-Te versus helical radius *u* showing "shifted" oscillator dynamics around new equilibrium positions (adapted from [23]).

deformation-potential e,h–phonon interaction (phonon part $|\Delta E_{res}^{ep}|$), respectively. In order to separate these contributions, one can mention that the pumping laser pulses are much shorter ($\tau_{pu}$(FWHM) ≈ 35 fs) than the phonon oscillation period $T_{ph} \approx 0.3$–0.4 ps (for the slightly damped phonon mode), i.e., $\tau_{pu}/T_{ph} \ll 1$. In this case, in the harmonic approximation the quasi-static displacement of ion sub-lattices, $U_{qs}$, equals to the amplitude $U_{osc}$ of sub-lattice oscillations around the new equilibrium position of the "shifted" oscillator ($|U_{qs}| = |U_{osc}|$) (Fig.6),[21] where the total phonon displacement is $U(t) = U_{qs}(t) + U_{osc}(t)$. This means that a quasi-static phonon-induced $|\Delta E_{res}^{qs}|$ component is equal to the amplitude, $|\Delta E_{res}^{osc}|$, of its oscillating counterpart $\Delta E_{res}^{osc}(t)$ (altogether $\Delta E_{res}^{qs}(t) + \Delta E_{res}^{osc}(t) = \Delta E_{res}^{ep}(t)$), while pedestals of the $\Delta E_{res}(t)$ curves in Figure 4 may be related to their fast electronic $\Delta E_{res}^{ee}(t)$ component. Such separation of $|\Delta E_{res}|$ into electronic and phonon components is supported by recent theoretical results,[7] showing the importance of both electronic

and phonon contributions during bandgap collapse in semiconductors. Note that the EHP Drude-like contributions to the dielectric functions $\varepsilon_{ord}$ and $\varepsilon_{ext}$ of the excited α-Te have been filtered out during the preceding fitting procedure.

Importantly, for the quite complicated structure of the top valence VB3 (*p*-lone-pair) band and the bottom conduction CB1 (*p*-antibonding) band including three sub-bands each[20] – see the band spectrum of electronically-excited α-Te in Figure 7 – $|\Delta E_{res}^{ee}|$ and $|\Delta E_{res}^{ep}|$ represent averages of individual bandgap renormalization sub-band shifts over the VB3, CB1 bands and over the *k*-space. As a result, one can consider $|\Delta E_{res}^{ep}| = \sum_{k'}[|\Delta E_{VB3,k'}^{ep}| + |\Delta E_{CB1,k'}^{ep}|] = \sum_{k'}\{|V_{VB3,k'}| + |V_{CB1,k'}|\}\cdot(|U_{qs}| + |U_{osc}|) = |V_{C/V,k'}|\cdot(|U_{qs}| + |U_{osc}|)$ and $|\Delta E_{res}^{ee}| = \sum_{k'}[|\Delta E_{VB3,k'}^{ee}| + |\Delta E_{CB1,k'}^{ee}|]$, where *k'* values represent particular regions of the *k*-space probed with the "ordinary" and "extraordinary" probe pulses, while $|V_{VB3,k'}|$, $|V_{CB1,k'}|$ and $|V_{C/V,k'}|$ correspond to the average valence band, conduction band, and overall optical deformation potentials, respectively.[22]

Transient shifts $\Delta E_{res,ext}(t)$ of the resonance energy $E_{res,ext} \approx$ 2.1 eV of the imaginary part of $\varepsilon_{ext}$ monitor time-dependent bandgap renormalization between CV1 and VB3 bands around the *A*-point of the band spectrum of α-Te (Fig.7). Their maximum values $|\Delta E_{res,ext}|$ separated into individual components $|\Delta E_{res,ext}^{ee}|$, $|\Delta E_{res,ext}^{osc}|$ and $|\Delta E_{res,ext}^{qs}|$, where $|\Delta E_{res,ext}| = |\Delta E_{res,ext}^{ee}| + |\Delta E_{res,ext}^{osc}| + |\Delta E_{res,ext}^{qs}|$ and $|\Delta E_{res,ext}^{osc}| = |\Delta E_{res,ext}^{qs}|$, are plotted in Figure 8 as functions of the "natural" variable $N_{e,h}$ using the calculated $N_{e,h}(F_{abs})$ dependence.[22] The resulting $|\Delta E_{res,ext}^{ee}|$ values of 0.05 – 0.12 eV for EHP densities in the range $(7 - 15)\cdot10^{20}$ cm$^{-3}$ are semi-quantitatively consistent with theoretical results for "electronic" bandgap renormalization in GaAs and Si, showing $\Delta E_g^{ee} \sim 0.1$ eV for $N_{e,h} \sim 10^{21}$ cm$^{-3}$.[7] Moreover, the $|\Delta E_{res,ext}^{ee}(N_{e,h})|$ curve in Figure 8 exhibits a linear slope $K^{ee}$, predicted in[7] to result for photo-excited GaAs at $N_{e,h} \geq 10^{21}$ cm$^{-3}$ from EHP-driven bandgap renormalization via screened-exchange electronic interactions. Our value of $K^{ee} = [0.95 \pm 0.03]\cdot10^{-22}$ eV·cm$^3$ shows that, similarly to GaAs,[7] for an excitation level of about 5% of $N_v$ in α-Te [$N_{e,h}(5\%) \approx 1\cdot10^{22}$ cm$^{-3}$], one can expect only a partial (50%) shrinkage of the average VB3-CB1 direct bangap in the *A*-point in this material ($\langle E_{g,k\approx A}\rangle \approx E_{res,ext} \approx 2$ eV) due to electronic screening, exchange and correlation effects. Further increase of $N_{e,h}$ in GaAs gives the opposite effect, where all bangaps start to open back because of electrostatic electron repulsion,[7] unambiguously stressing the high importance of the deformation-potential e,h–phonon interaction in bandgap renormalization in highly-excited semiconductors.

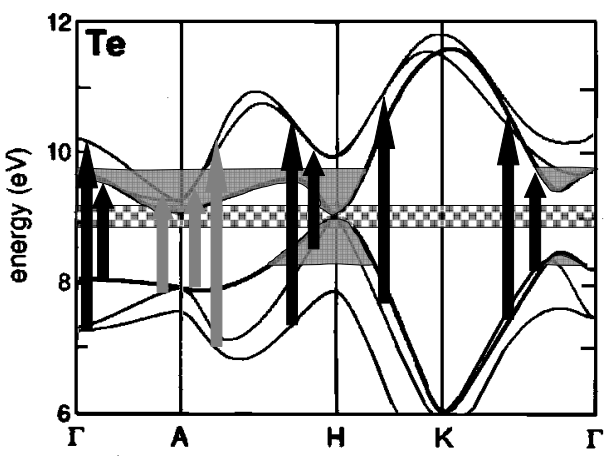


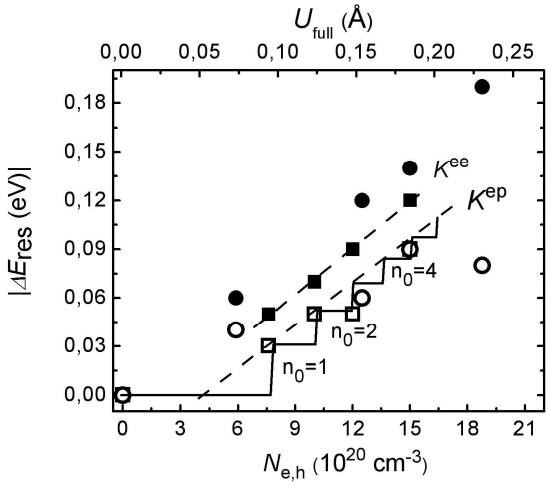


Fig. 7 (left). Renormalized spectrum of VB3 and CB1 bands in α-Te (after[20,23]) and its regions probed in this work using probe pulse polarizations $\boldsymbol{E}_{pr} \parallel \boldsymbol{c}$ (grey arrows) and $\boldsymbol{E}_{pr} \perp \boldsymbol{c}$ (black arrows). Short and long arrows correspond to 1.65-eV ($\approx \hbar\omega_{pu}$) and 3.2-eV probe photons respectively, showing the probed energy range. Population of conduction and valence bands by free carriers at their maximum achieved temperature $k_B T_{e,h} \approx 0.28$ eV[22] is shown by coloring corresponding valleys in grey, while the initial *H*-point direct bandgap (0.33 eV) is shown schematically by the speckled band..

Fig. 8 (right). Transient absorption resonance shifts $|\Delta E_{res,ext}^{ee}|$ (solid circles), $|\Delta E_{res,ord}^{ee}|$ (solid squares), $|\Delta E_{res,ext}^{qs}|$ (open circles) and $|\Delta E_{res,ord}^{qs}|$ (open squares) vs. $N_{e,h}$ (bottom axis) and phonon amplitude $U_{full}$ (top axis). The step-like curve represents the fitting function $\Delta E_{res,k\approx A}(U_{full})$ and the two straight lines exhibit slopes $K^{ee}$ and $K^{ep}$. Dashed curves demonstrate linear dependence of $|\Delta E_{res,ext}^{ee}|$ and $|\Delta E_{res,ext}^{qs}|$ on $N_{e,h}$ predicted by theory[7,22].

In contrast, transient resonance energy shifts $\Delta E_{res,ord}(t)$ measured for $\varepsilon_{ord}$ where $E_{res,ord} \approx 2.3$ eV, are tracking the average bandgap renormalization over the *k*-space of the first Brillouine zone of α-Te, excluding just the region adjacent to the *A*-point, i.e., in *Γ*, *H*, *L* and *M* points (Fig.7).[20] The electronic maximum bandgap renormalization component, $|\Delta E_{res,ord}^{ee}|$, when represented vs. $N_{e,h}$ (Fig.8), appears as a linear curve nearly coinciding with the $|\Delta E_{res,ext}^{ee}(N_{e,h})|$ curve. Therefore, one can conclude that: *i*) the electronic bandgap renormalization in α-Te is nearly isotropic and homogeneous (at least, for optically probed electronic states separated by $E_g \approx 1.5 - 3.2$ eV) due to the high site symmetry of carrier-carrier interactions (in agreement with theoretical results in[7]), *ii*) the above described procedure of evaluating $N_{e,h}$ under "extraordinary" excitation conditions seems to be valid. Importantly, these $|\Delta E_{res,ext}^{ee}(N_{e,h})|$ and $|\Delta E_{res,ord}^{ee}(N_{e,h})|$ curves represent the first experimental quantitative measurements of electronic bandgap renormalization vs. $N_{e,h}$ in α-Te and other semiconductors, encouraging further theoretical studies of many-particle electronic effects in such materials.

The quasi-static phonon component of $|\Delta E_{res,ext}|$, represented in Figure 8 by the $|\Delta E_{res,ext}^{qs}(N_{e,h})|$ curve, exhibits a nearly linear increase with $N_{e,h}$, predicted by theory.[22] Its slope $K^{ep} = (0.8 \pm 0.1)\cdot 10^{-22}$ eV·cm$^3$ is very close to $K^{ee}$, showing the high importance of the deformation-potential e,h–phonon interaction during bandgap renormalization of the *A*-point band spectrum in α-Te. According to the $K^{ep}$ value, coherent optical phonons provide the same 50% shrinkage of the average *A*-point direct VB3–CB1 bangap, $\langle E_{g,k\approx A}\rangle$, for the 5% excitation level, corresponding, together with the $|\Delta E_{res,ext}^{ee}|$ contribution, to a total collapse of the bandgap and an insulator-metal transition. The 5% threshold for the insulator-metal transition, $[N_{e,h}(5\%) \approx N_{BG,k\approx A}]$, is close to well-known theoretical lattice instability and metallization thresholds of about 10% of $N_v$ in other semiconductors.[24]

Furthermore, there is an intriguing large horizontal offset $\approx 3\cdot 10^{20}$ cm$^{-3}$, of the linear curve fitting the $|\Delta E_{res,ext}^{qs}(N_{e,h})|$ dependence in Figure 8, which is comparable to the EHP densities achieved here. Simultaneously, this linear curve, when extrapolated to $N_{e,h} = 0$, shows a large vertical offset $\approx -0.03$ eV, comparable to the intervals between the $|\Delta E_{res,ext}^{qs}|$ data points of the curve. Both these offsets may be explained by pronounced quantization of $|\Delta E_{res,ext}^{qs}|$ at small phonon numbers $n_0$, corresponding to $N_{e,h}$ values close to the EHP density threshold for EHP-driven emission of the first coherent $A_1$-optical phonon, because of a quantum character of both the coherent optical phonon displacements, $|U_{qs}(n_0)| = |U_{osc}(n_0)| \approx (2n_0)^{1/2}U_0$, when described in the "shifted oscillator" approximation at $\tau_{pu}/T_{ph} \ll 1$.[21] Therefore, the $|\Delta E_{res,ext}^{qs}|$ data can be represented well, i.e. without any offsets, vs. the full coherent optical phonon amplitude $U_{full} = (2n_0+1)^{1/2}U_0$ including the zero-energy oscillation ($n_0 = 0$) amplitude $U_0 \approx 5.6$ pm[22] in α-Te (top axis in Fig.8) by a step-like function $\Delta E_{res,k\approx A}^{qs}(U_{full}) = (|V_{C,k\approx A}| + |V_{V,k\approx A}|)\cdot[U_{full} - U_0]$. The slope of the linear $\Delta E_{res,k\approx A}^{qs}(U_{full})$ curve in Figure 8, which represents a module of the "effective" CB1/VB3 intraband optical deformation potential $|V_{C/V,k\approx A}| = |V_{CB1,k\approx A}| + |V_{VB3,k\approx A}| = 0.7 \pm 0.1$ eV/Å, equals to the average of the *A*-point intraband optical deformation potential moduli of those CB1 and VB3 sub-bands, which are allowed for optical probing in accordance with the corresponding selection rules, while the difference $[U_{full}-U_0]$ equals to $U_{qs}(n_0) = U_{osc}(n_0)$ and the deformation-potential e,h–phonon interaction is absent, by its definition, at $n_0 = 0$.

Likewise, one can represent the data of the $|\Delta E_{res,ord}^{qs}(N_{e,h})|$ curve in Figure 8 in the form $\Delta E_{res,k\text{-}A}(U_{full}) = (|V_{C,k\text{-}A}| + |V_{V,k\text{-}A}|)\cdot[U_{full} - U_0]$, where the slope $|V_{C/V,k\text{-}A}| = |V_{CB1,k\text{-}A}| + |V_{VB3,k\text{-}A}|$ corresponds to the "effective" CB1/VB3 intraband optical deformation potential and represents the electronic states over the entire *k*-space, with an exception of the *A*-point region, accounting for selection rules for optical probing of these states near the *Γ*, *H*, *L* and *M* points. As expected from the similarity between the slopes of the $|\Delta E_{res,ext}^{qs}(N_{e,h})|$ and $|\Delta E_{res,ord}^{qs}(N_{e,h})|$ curves in Figure 8, the value $|V_{C/V,k\text{-}A}| = 0.6 \pm 0.2$ eV/Å is in close agreement with $|V_{C/V,k\approx A}| = 0.7 \pm 0.1$ eV/Å. Also, the slope of the $|\Delta E_{res,ord}^{qs}(N_{e,h})|$ curve, $(0.8 \pm 0.2)\cdot 10^{-22}$ eV·cm$^3$ (not shown in Fig.8), shows that the total collapse of the average direct VB3-CB1 bangap, $\langle E_{g,k\text{-}A}\rangle \approx E_{res,ord}$, takes place at $N_{BG,k\text{-}A} \approx 1.2\cdot 10^{22}$ cm$^{-3}$, i.e., at 6% photoexcitation level, including both the electronic and phonon-induced bandgap renormalization effects.

Finally, the oscillatory and quasi-static coherent phonon displacements $U_{qs}$ and $U_{osc}$ have been directly obtained as a function of $N_{e,h}$ curve (Fig.9) from the experimental curves of $|\Delta E_{res,ext}^{qs}|$ and $|\Delta E_{res,ord}^{qs}|$ vs $N_{e,h}$ calculating, e.g., the $|\Delta E_{res,ext}^{qs}(N_{e,h})|/|V_{C/V,k\approx A}|$ ratio. This curve is in good agreement with the theoretical one calculated using DFT method.[23] It shows that single – from one to four – $A_1$-phonons have been discretely emitted in α-Te under electronic excitation conditions of this work demonstrating absolute detection capabilities of our technique in studies of coherent phonon dynamics in solids.

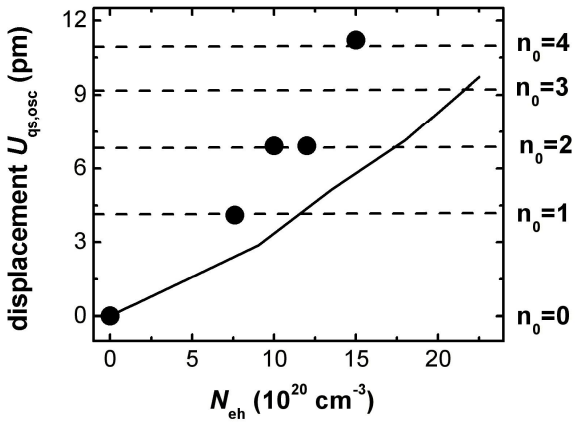


Fig. 9. Quantized picometer phonon displacements $U_{qs,osc}$ in α-Te at different phonon occupation numbers $n_0$ versus $N_{e,h}$: dark circles – extraordinary set of data of this work, solid line – data after[23].

## IV. CONCLUSIONS

In conclusion, by means of time-resolved optical reflectometry we have measured transient sub-picosecond picometer atomic sub-lattice displacements in α-Te (amplitudes in the range of 4-10 pm) photo-excited by single femtosecond laser pulses. These displacements represent the small number – one to four – of coherent softened fully symmetrical optical $A_1$-phonons discretely emitted as a function of the increasing electronic excitation level. These measurements demonstrate that the absolute detection limit – observation of a single coherent phonon – has been achieved, together with the high temporal resolution, in this study of coherent phonon dynamics in solids.

## ACKNOWLEDGEMENTS

This work was supported by a grant No. DMR-0303642 to E. Mazur from the National Science Foundation.

## REFERENCES

1. H.J. Zeiger, J. Vidal, T.K. Cheng, E.P. Ippen, G. Dresselhaus, M.S. Dresselhaus, Phys. Rev. B **45**, 768 (1992).
2. S. Hunsche, K. Wienecke, T. Dekorsy, H. Kurz, Phys. Rev. Lett. **75**, 1815 (1995); S. Hunsche, H. Kurz, Appl. Phys. A **65**, 221 (1997).
3. A.M.-T. Kim, C.A.D. Roeser, E. Mazur, Phys. Rev. B **68**, 012301 (2003); C.A.D. Roeser, M. Kandyla, A. Mendioroz and E. Mazur, Phys. Rev. B **70**, 212302 (2004).
4. K. Sokolowski-Tinten, C. Blome, J. Blums, A. Cavalleri, C. Dietrich, A. Tarasevitch, I. Uschmann, E. Forster, M. Kammler, M. Horn-von Hoegen, D. von der Linde, Nature **422**, 287 (2003).
5. M. Hase, M. Kitajima, S. Nakashima, K. Mizoguchi, Phys. Rev. Lett. **88**, 067401 (2002); M. Hase, K. Ishioka, J. Demsar, K. Ushida, M. Kitajima, Phys. Rev. B **71**, 184301 (2005).
6. H.J. Zeiger, T.K. Cheng, E.P. Ippen, J. Vidal, G. Dresselhaus, M.S. Dresselhaus, Phys. Rev. B **54**, 105 (1996); M.F. DeCamp, D.A. Reis, P.H. Bucksbaum, R. Merlin, Phys. Rev. B **64**, 092301 (2001).

7. C.S. Spataru, L.X. Benedict, S.G. Louie, Phys. Rev. B **69**, 205204 (2004); see also A. Oschlies, R.W. Godby, R.J. Needs, Phys. Rev. B **45**, 13741 (1992) and D.H. Kim, H. Ehrenreich, E. Runge, Sol. State Commun. **89**, 119 (1994).
8. R.E. Peierls, *Quantum theory of solids* (Oxford, Clarendon Press, 1955), Ch.5; R.E. Peierls, *More surprises in theoretical physics* (Princeton, Princeton University Press, 1991), Ch.2.
9. P.B. Hillyard, K.J. Gaffney, A.M. Lindenberg *et al*., Phys. Rev. Lett. **98**, 125501 (2007).
10. B.J. Siwick, J.R. Dwyer, R.E. Jordan, R.J.D. Miller, Science **302**, 1382 (2003).
11. U. Bovensiepen, A. Melnikov, I. Radu, O. Krupin, K. Starke, M. Wolf, E. Matthias, Phys. Rev. B **69**, 235417 (2004).
12. P.A. Loukakos, M. Lisowski, G. Bihlmayer *et al*., Phys. Rev. Lett. **98**, 097401 (2007).
13. C. A. D. Roeser, A. M.-T. Kim, J. P. Callan, L. Huang, E. N. Glezer, Y. Siegal, E. Mazur, Rev. Sci. Instrum. **74**, 3413 (2003).
14. S. Backus, J. Peatross, C. P. Huang, M. M. Murnane, H. C. Kapteyn, Opt. Lett. **20**, 2000 (1995).
15. T. F. Albrecht, K. Seibert, H. Kurz, Opt. Commun. **84**, 223 (1991).
16. S. A. Kovalenko, A. L. Dobryakov, J. Ruthmann, N. P. Ernsting, Phys. Rev. A **59**, 2369 (1999).
17. C.A.D. Roeser, PhD thesis, Harvard University, 2003.
18. E.D. Palik (ed.), *Handbook of Optical Constants of Solids* (Academic Press, San Diego, 1991).
19. N. W. Ashcroft, N. D. Mermin, *Solid State Physics* (Saunders College, Philadelphia, 1976).
20. Landolt-Bornstein, *Numerical data and functional relationships in science and technology*, New Series, V. III 41, Semiconductors C: Non-Tetrahedrally Bonded Elements and Binary Compounds I, Editor: O. Madelung, (Springer-Verlag, Berlin, 1998).
21. A.V. Kuznetsov, C.J. Stanton, Phys. Rev. Lett. **73**, 3243 (1994).
22. S.I. Kudryashov, M. Kandyla, C. Roeser, E. Mazur, Phys. Rev. B **75**, 085207 (2007).
23. P. Tangney, M.Sc. thesis, University College (Cork), 1998; P. Tangney, S. Fahy, Phys. Rev. Lett. **82**, 4340 (1999); P. Tangney, S. Fahy, Phys. Rev. B **65**, 054302 (2002).
24. P. Stampfli, K.H. Bennemann, Phys. Rev. B **49**, 7299 (1994); J.S. Graves, R.E. Allen, Phys. Rev. B **58**, 13627 (1998); V.I. Emel'yanov, D.V. Babak, Phys. Solid State **41,** 1338 (1999).